Materials Research Proceedings 44 (2024) 519-527 https://doi.org/10.21741/9781644903254-56

The influence of process parameters on the axial force of the continuous rolling section in the synchronous forming process of shape and inner hole for hollow axles

YE Caoqi[1,a], SHU Xuedao[1,b*], WANG Jitai[1,c], XIA Yingxiang[1,d], LI Zixuan[1,e] and XU Haijie[1,f]

[1]Ningbo University No. 818 Fenghua Road, Jiangbei District, Ningbo, Zhejiang Province, China

[a]yecaoqi925@gmail.com, [b]shuxuedao@nbu.edu.cn, [c]wangjitai0708@gmail.com, [d]xiayingxiangnbu@163.com, [e]lizixuan@nbu.edu.cn, [f]xuhaijie@nbu.edu.cn

Keywords: Process Parameters, FEM, Synchronous Forming, Axial Stress, Hollow Axle

Abstract. To verify the feasibility of the synchronized forming of shape and inner hole for hollow axles and the influence of process parameters on the axial force in the continuous rolling section, a finite element model of the synchronized forming of shape and inner hole for hollow axles was established using finite element analysis software, and the forming process of hollow axle shafts was simulated. The results indicate that synchronized forming with shaped holes for hollow axle shafts is feasible. The axial stress in the continuous rolling section increases with the feed angle of the piercing roll. With the increase in the speed of the piercing roll, the axial stress in the continuous rolling section shows a trend of rapid increase followed by a slow increase. Moreover, as the conical angle of the disc-shaped rolls increases, the axial stress in the continuous rolling section generally increases.

Introduction

The hollow axle is a core component of high-speed trains. Compared with traditional solid axles, it has advantages such as reducing the mass below the spring, reducing the force between the wheel and the rail, and facilitating ultrasonic flaw detection. However, its higher production cost and technical barriers have led to a single manufacturing technology for hollow axles, cumbersome production processes, and key technologies being monopolized by a few companies. In recent years, many scholars have conducted extensive research on new hollow axle production technologies. Zheng Shuhua et al. analyzed the stable rolling conditions of the cross wedge rolling of hollow axles and obtained criteria for determining the instability of cross wedge rolling of hollow axles. They analyzed the effects of spread angle and forming angle on the thickness uniformity and obtained the regularity of the influence of process parameters on the thickness of hollow axles rolled by cross wedge rolling [1]. Shuexuedao et al. studied the influence of die process parameters on the energy parameters of cross wedge rolling of hollow axles [2]. Xu Chang et al. simulated the forming process of hollow axles by three-roll skew rolling using finite element software. They analyzed the metal flow law, strain field, temperature field, and variation law of rolling force in this process, elucidating the forming mechanism of hollow axles by three-roll skew rolling and the influence of process parameters on mechanical parameters [3,4]. Pater et al. successfully rolled reduced-scale solid axles on a CNC three-roll skew rolling machine, confirming that axle shafts of rail vehicles can be formed by the three-roll skew rolling process. They also explored the influence of process parameters on the occurrence of spiral thread defects in the transition section of hollow axles and discussed the impact of spiral threads on the quality of axle cores, finding that this defect does not significantly affect the core quality [5,6]. Romanenko V.P. et al. proposed a manufacturing technology for hollow axles using rotary tube piercing to form inner holes and radial forging technology to form outer shapes. They tested the mechanical

properties of hollow axles manufactured using this process [7-8].The introduction of these new hollow axle forming technologies has enriched the manufacturing technology of hollow axles and provided new ideas for their production.

The above-mentioned new technologies cover plastic forming methods such as cross wedge rolling, skew rolling and forging, exploring exploratory forming of hollow axles by utilizing the strengths of various processes. Inspired by previous research, this study innovatively proposes the hollow axle synchronous forming process, as shown in Fig. 1. The rolling process of this technology is as follows: firstly, the billet reaches the deformation zone of the perforation section under the pushing of the plunger and is bitten by the piercing rolls. After passing through the perforation deformation zone, the billet becomes a tube, which then enters the rolling deformation zone and is bitten by the disc rolls. The tube is rolled into a stepped shaft with certain dimensions by the radial movement of the disc rolls. After the entire billet passes through the piercing zone, the clamp behind the disc rolls bite the rolled piece and moves axially at a certain speed coordinated with the radial speed of the disc roll until the rolling is completed.

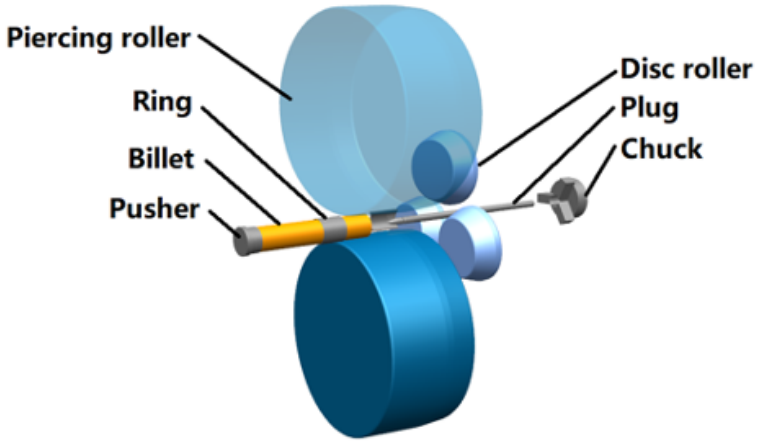

Fig. 1. Principle of synchronous forming of hollow axle.

Compared with traditional technologies for producing hollow axles, this technology improves the forming efficiency and material utilization of hollow axles, and reduces the footprint of equipment, as both external and internal shaping can be performed on a single mill. As this process shares characteristics with continuous rolling processes, analyzing the stress state of the hollow axle's rolling segment and the influence of process parameters on its stress state is a key issue in this technology. Therefore, this study conducts finite element simulations of the process and investigates the effects of piercing roll speed, feed angle α1 of piercing roll , and cone angle β of disc roll (as shown in Fig. 2) on the axial force of the rolling segment of hollow axles.

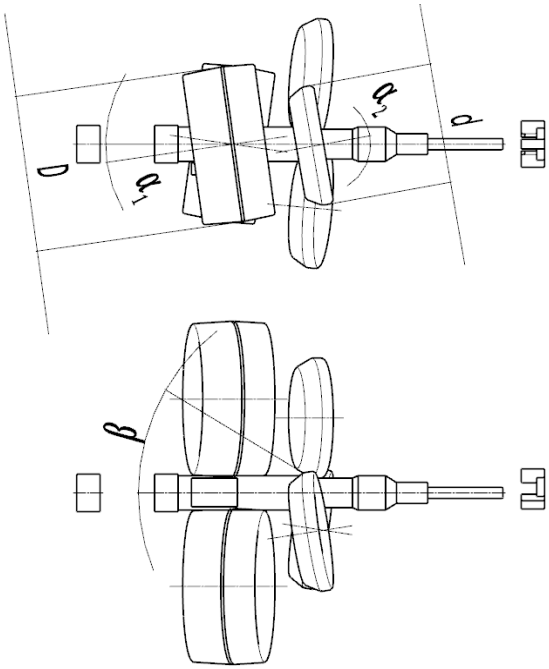

Fig. 2. Projection diagram of this process.

Establishment of Finite Element Model and Analysis of the Process

Hot Compression Behavior of 30NiCrMoV12

Hot Compression Test. To investigate the high-temperature flow behavior of 30NiCrMoV12 during thermal plastic deformation and to construct a more reliable numerical simulation model, a hot compression test plan for 30NiCrMoV12 was developed in conjunction with the process characteristics of skew rolling forming. High-temperature flow stress curves under different conditions were obtained, and the influence of deformation parameters on the high-temperature deformation behavior of 30NiCrMoV12 was analyzed. The high-temperature uniaxial compression tests were conducted on a Gleeble-3500 thermal simulation machine, using cylindrical specimens with dimensions of φ8 mm × 12 mm. Before deformation, tantalum chips were attached to both ends of the specimen to reduce friction between the specimen and the compression head. After securing the specimen, it was heated to the preset temperature at a rate of 5 ℃/s and held for 3 minutes to reach thermal equilibrium. Subsequently, the specimen was compressed to a deformation of 50% at the preset strain rate, followed by immediate water quenching upon completion of compression deformation. The process of high-temperature uniaxial compression testing is illustrated in Fig. 3.

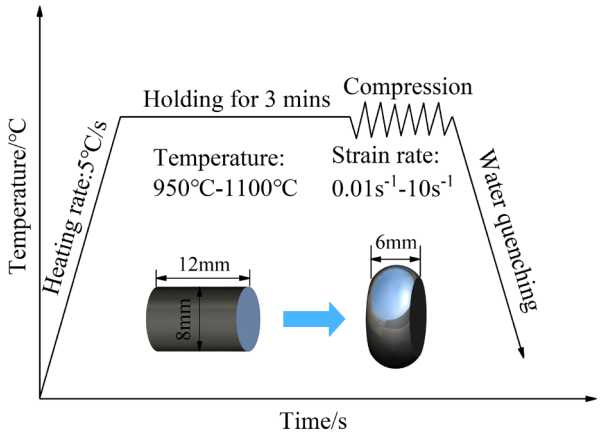

Fig. 3. Process of high-temperature uniaxial compression testing.

Hot Compression Test Results. Fig. 4 shows the stress-strain curves of 30NiCrMoV12 under different high-temperature deformation conditions. It can be observed from the graph that the stress under different deformation conditions increases sharply and reaches a peak within a very small strain range. This is attributed to the generation, intersection, and entanglement of dislocations causing work hardening, leading to a rapid increase in flow stress. As deformation continues to increase, dynamic recovery rearranges, slips, and annihilates accumulated dislocations, resulting in a decreasing trend or reduction in the increase of flow stress [9]. Moreover, when microstructural changes occur within the material, such as recrystallization and dynamic recrystallization, the flow softening rate caused can further counteract the hardening rate, leading to a decrease in flow stress or reaching a steady state [10]. Therefore, plastic deformation of the material is a process where hardening and softening mechanisms coexist and compete, and this process exhibits strong temperature and strain rate sensitivity.

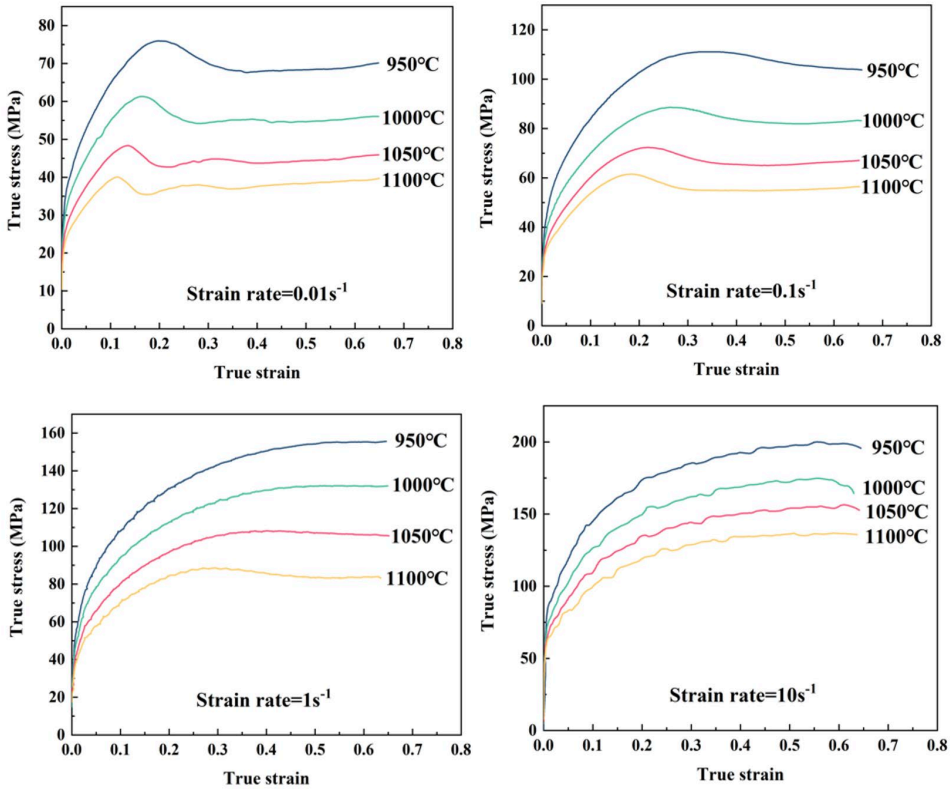

Fig. 4. Stress-strain curves of 30NiCrMoV12 under different high-temperature deformation conditions.

Establishment of the Constitutive Model for 30NiCrMoV12. Based on the Arrhenius constitutive model, the measured flow stress data from the hot compression experiments of 30NiCrMoV12 are subjected to multivariate regression analysis, resulting in the following constitutive equation:

$$\dot{\varepsilon} = 7.05\times10^{11}[\sinh(0.009832\sigma_{\mathrm{p}})]^{4.66}\exp\left(-\frac{314505}{RT}\right) \quad (1)$$

Where: $\dot{\varepsilon}$ is the strain rate, σ_p is the yield stress, R is the gas constant, and T is the temperature.

Finally, the obtained constitutive equation is imported into the material library of finite element software using secondary development software to provide a more accurate material model for finite element analysis.

Establishment of Finite Element Model. Fig. 5 illustrates the finite element model of synchronous forming of 30NiCrMoV12 axle-shaped holes established in this study using the FORGE NxT 1.1 software. The parameter settings and boundary conditions of this model are as follows: During the rolling process, the workpiece undergoes severe plastic deformation, and its elastic deformation can be neglected. The rolling rolls and guides undergo minimal deformation, thus the workpiece is set as rigid-plastic, and the rolling rolls and guides are set as rigid bodies. The rolling rolls rotate about the inner diameter center axis, driven by a motor, and the rotational speed is set according to the rolling conditions. A shear friction model commonly used to describe volume forming friction conditions is selected to describe the friction between the workpiece and the rolling rolls during contact. The friction factor between the workpiece and the rolling rolls is set to 0.8.The contact thermal conductivity coefficient between the workpiece and the rolling rolls/guides is set to 25,000 W/(m·K), and the convective heat transfer coefficient between the workpiece and air is set to 20 W/(m·K).

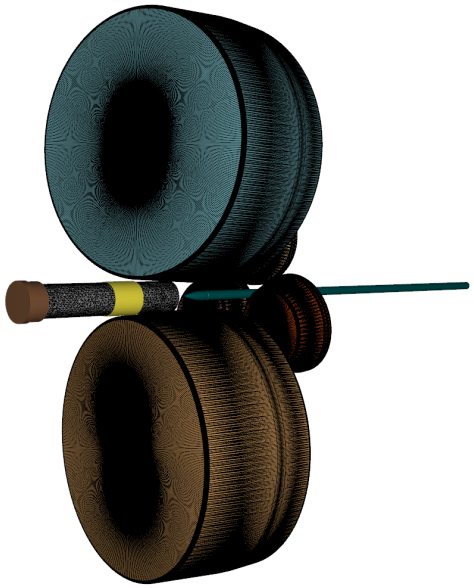

Fig. 5. Finite element model of the process.

The finite element simulation process is illustrated in Fig. 6. From the diagram, it can be observed that the billet is first pierced to form a hollow tube in the piercing section. Subsequently, the hollow tube is rolled into a stepped shaft with certain dimensions in the continuous rolling section. This process eliminates the need for reheating the hollow tube, saving energy and time, which is highly beneficial for metals with a narrow rolling temperature range. From the final formed shape, it can be seen that apart from the material head at the tail end of the axle and the spiral threads on the surface of the long axle section, which need to be removed by machining, the dimensions of the remaining parts are very close to those of standard axles. Therefore, forming a hollow axle using this process is feasible.

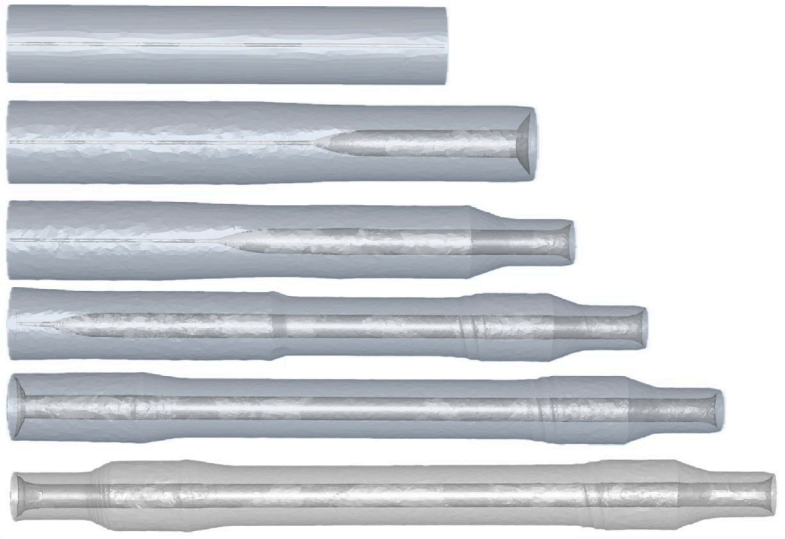

Fig. 6. Finite element simulation process.

The Influence of Process Parameters on Axial Force in the Continuous rolling section

The synchronized forming of shape and inner hole for hollow axles process can shape both the inner hole and the outer shape of the axle on a single rolling mill. During this process, two sets of rolls simultaneously act on the billet. Therefore, the working conditions of these two sets of rolls need to satisfy certain continuous rolling relationships to ensure the smooth progress of the rolling process. The stress state of the billet between the two sets of rolls during the rolling process is the key issue we need to study. The billet in the continuous rolling section is subjected to circumferential forces from the piercing roll and the disc roll, which cause it to rotate, as well as axial forces that induce axial movement. The magnitude of these two forces determines whether the rolling process can proceed smoothly. Therefore, in the following discussion, the axial force is selected as the research object, and the influence of the piercing roll feed angle, piercing roll speed, and disc roll cone angle on the axial force is investigated. The selection of process parameters is shown in Table 1.

Table 1. Selection of process parameters.

Condition	piercing roll feed angle[°]	piercing roll speed[rpm]	disc roll cone angle[°]
1	4/5/6/7	20	20
2	5	17/20/23/26	20
3	5	20	15/20/25/30

In order to obtain the magnitude of the axial stress in the continuous rolling section during the rolling process, three tracking points are selected at the exit of the piercing section. The method for selecting the tracking points is shown Fig. 7. The axial stress of these three points from the exit of the piercing section to the entrance of the continuous rolling section is recorded. Then, the average axial stress of the three points is taken as the axial stress value of the continuous rolling section under this process parameter.

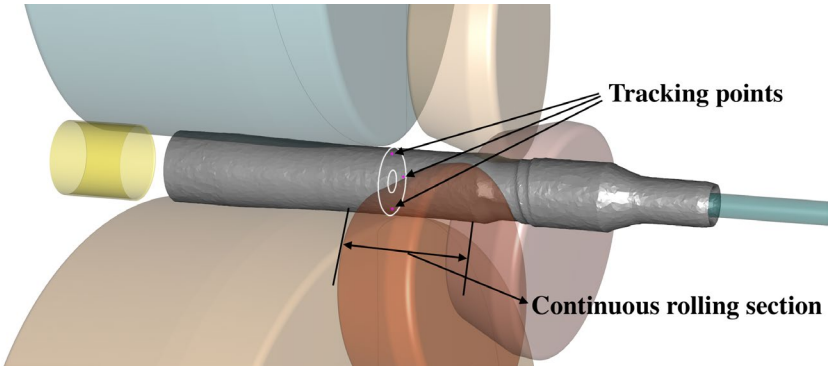

Fig. 7. Selecting of the tracking points.

The influence of piercing roll feed angle. The variation in axial stress magnitude in the continuous rolling section under different piercing roll feed angles is shown in Fig. 8. From the graph, it can be observed that the axial stress experienced by the continuous rolling section is compressive stress. This indicates that the axial velocity imparted to the billet by the piercing roll is greater than the axial velocity imparted by the disc roll during the rolling process. This is because, with the same circumferential speed of the rolls, the axial component of the rolling force exerted by the piercing roll on the billet is greater than the axial component of the rolling force exerted by the disc roll. Furthermore, the graph shows that the axial stress in the continuous rolling section increases with an increase in the piercing roll feed angle. This is attributed to the increase in the axial velocity component of the rolls with the increase in the piercing roll feed angle. Consequently, the axial velocity imparted to the billet by the piercing roll increases due to frictional forces. However, under this circumstance, the axial velocity imparted to the billet by the disc roll does not increase, directly leading to an increase in the axial stress in the continuous rolling section.

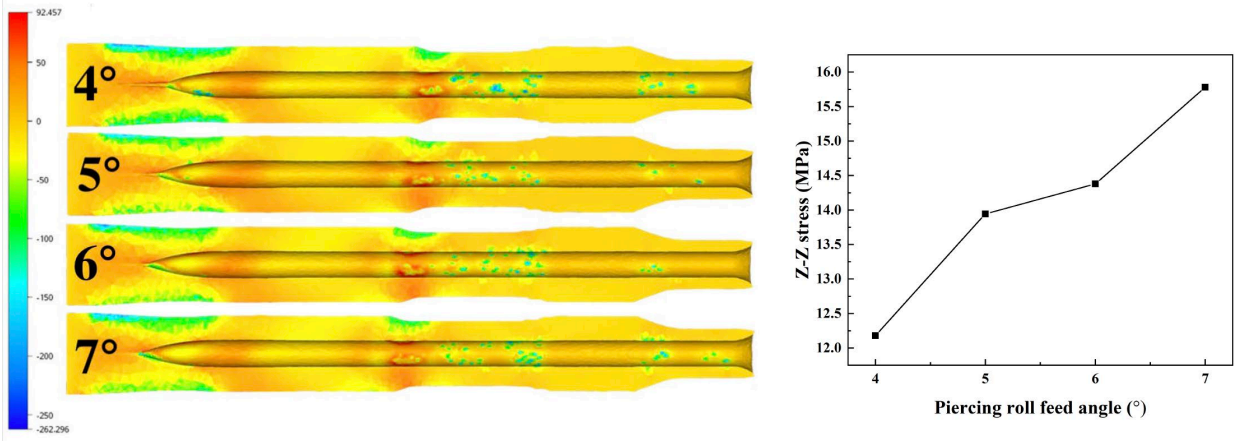

Fig. 8. The variation in axial stress magnitude in the continuous rolling section under different piercing roll feed angles.

The influence of piercing roll speed. Fig. 9 depicts the variation in axial stress in the continuous rolling section under different piercing roll speeds. From the graph, it can be observed that the axial stress experienced by the continuous rolling section during the rolling process remains compressive. Moreover, with an increase in the piercing roll speed, the axial stress in the continuous rolling section exhibits a trend of rapid increase followed by a gradual increase. The primary reason for the increase in axial stress is the increasing difference in axial velocities between the billet in the piercing section and the continuous rolling section. However, after the piercing roll speed reaches 20 rpm, the rate of increase in axial stress slows down. This phenomenon can be attributed to the following reasons: With the increase in roll speed, the material's strain rate increases, and the friction between the rolls and the billet becomes more

intense. This leads to a rise in the billet's temperature. The increase in billet temperature has a softening effect on the material, causing the rate of increase in axial stress to decrease. Therefore, while the difference in axial velocities contributes to the increase in axial stress, the softening effect induced by the rise in billet temperature mitigates the rate of increase in axial stress beyond a certain roll speed.

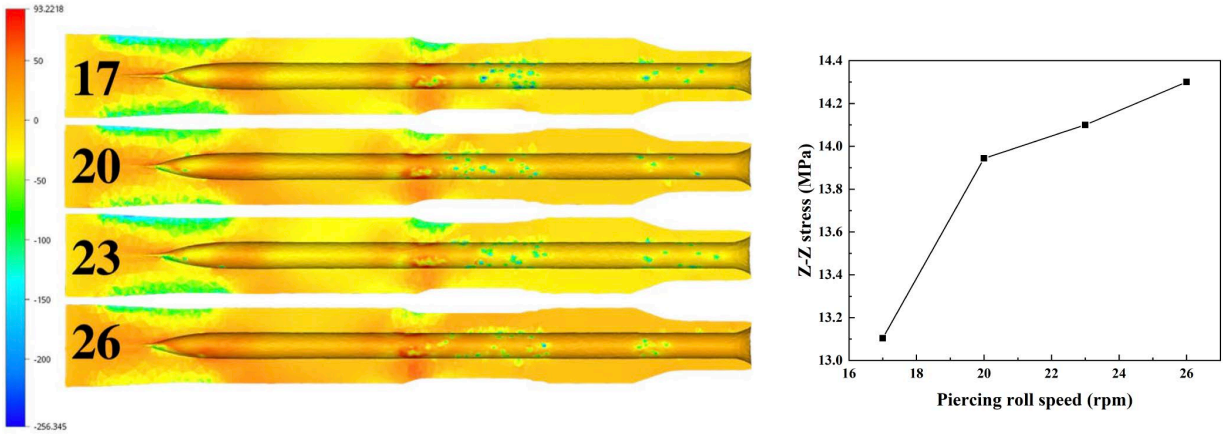

Fig. 9. The variation in axial stress magnitude in the continuous rolling section under different piercing roll speed.

The influence of disc roll cone angle. Fig. 10 illustrates the influence of different cone angles of the disc rolls on the axial stress in the continuous rolling section. From the graph, it can be observed that as the cone angle of the disc rolls increases, the overall trend of the axial stress in the continuous rolling section is an increase. This is because, with the increase in cone angle, the contact area between the disc rolls and the billet decreases. Consequently, this directly leads to a reduction in the rolling force exerted on the continuous rolling section. As a result, the axial velocity of the continuous rolling section decreases. This, in turn, increases the difference in axial velocities between the billet in the piercing section and the continuous rolling section, thereby causing an increase in axial stress in the continuous rolling section.

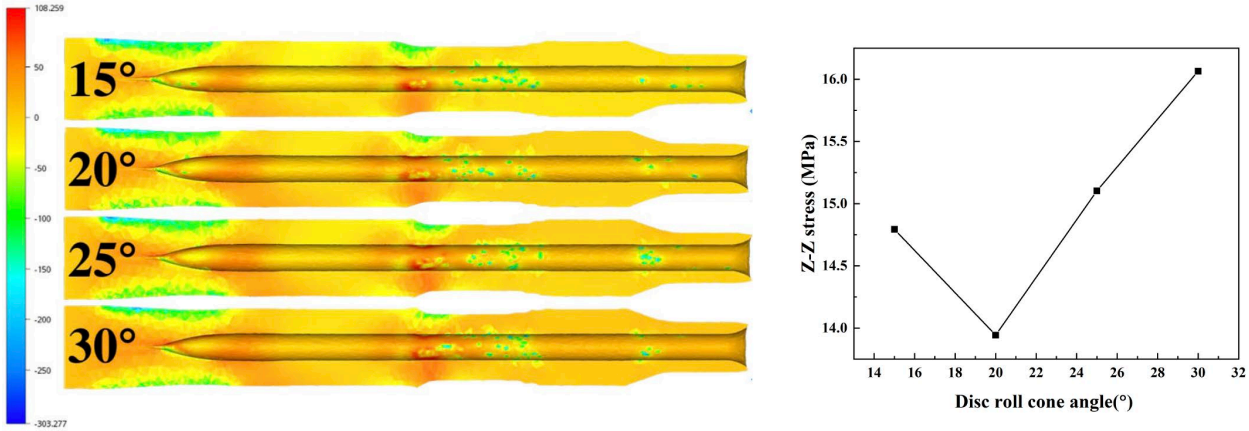

Fig. 10. The variation in axial stress magnitude in the continuous rolling section under different disc roll cone angles.

Conclusion

1. The synchronized forming of shape and inner hole for hollow axles process is feasible. It can effectively increase material utilization and rolling efficiency.
2. The axial stress in the continuous rolling section increases with an increase in the piercing roll feed angle. Additionally, with an increase in piercing roll speed, the axial stress in the continuous

rolling section exhibits a trend of rapid increase followed by a gradual increase. Moreover, as the cone angle of the disc rolls increases, the axial stress in the continuous rolling section shows an overall increasing trend.

Funding
This study was funded by the Natural Science Foundation of Zhejiang, China (Grant Number: LZ22E050002), the National Natural Science Foundation of China (Grant Number: 51975301), and the Major Project of Science and Technology Innovation 2025 in Ningbo City, China (Grant Number: 2022Z064, 2022Z009, 2022Z015).

References

[1] S.H. Zheng, X.D. Shu, B.S. Sun, W.F. Peng, Wall thickness uniformity of railway hollow shafts by cross-wedge rolling. Chin. J. Eng, 37 (2015) 648-654. https://doi.org/10.13374/j.issn2095-9389.2015.05.017

[2] X.D. Shu, C. Liu, B.S. Sun, W.F. Peng, P.H. Yu, Influence of mold technological parameters on the forming force parameters in multi-wedge rolling of the railway hollow shafts. J. Plast. Eng. 23 (2016) 23-28. https://doi.org/10.3969/j.issn.1007-2012.2016.03.005

[3] C. Xu, X.D. Shu, Y. Zhu, Simulation and analysis of three-roll skew rolling forming of the railway hollow shaft. J. Ningbo Univ. NSEE 31 (2018) 16-19.

[4] C. Xu, X.D. Shu, Influence of process parameters on the forming mechanics parameters of the three-roll skew rolling forming of the railway hollow shaft with 1 : 5, Metalurgija 57(2018) 153 -156.

[5] Z. Pater, J. Tomczak, K, Lis, T. Bulzak, X.D. Shu, Forming of rail car axles in a CNC skew rolling mill, Arch. Civ. Mech. Eng. 20 (2020) 1-13. https://doi.org/10.1007/s43452-020-00075-5

[6] Z. Pater, J. Tomczak, T. Bulzak, Problems of forming stepped axles and shafts in a 3-roller skew rolling mill, J. Mater. Res. Technol. 9 (2020) 10434-10446. https://doi.org/10.1016/j.jmrt.2020.07.062

[7] V.P. Romanenko, B.A. Romantsev, G.P. Illarionov, Billet Preparation Method for Railcar Hollow Axle Production, Metallurgist 58 (2014) 684-688. https://doi.org/10.1007/s11015-014-9977-0

[8] V.P. Romanenko, P.P. Stepanov, S.M. Kriskovich, Production of Hollow Railroad Axles by Screw Piercing and Radial Forging, Metallurgist 61 (2018) 873-877. https://doi.org/10.1007/s11015-018-0579-0

[9]Z.L. Liu, S. Ren, W. Liu, Hot deformation behavior and microstructure evolution of GH141 nickel-based superalloy, The Chinese J. Nonferrous Met. 33 (2023) 2577-2592. https://doi.org/10.11817/j.ysxb.1004.0609.2022-43577

[10]W.W. Zhang, X.G. Liu, H.Z. Li, Study on microstructure evolution of GH4742 alloy underthermo-mechanical coupling based on LAM technology, J. Mech. Eng. 58 (2022) 110-120. https://doi.org/10.3901/JME.2022.16.110